Experiments with Ξ^- atoms

C.J. Batty[1], E. Friedman[2], and A. Gal[2]
[1]Rutherford Appleton Laboratory, Chilton, Didcot, Oxon, OX11 0QX, UK
[2]Racah Institute of Physics, The Hebrew University, Jerusalem 91904, Israel

Abstract

Experiments with Ξ^- atoms are proposed in order to study the nuclear interaction of Ξ hyperons. The production of Ξ^- in the (K^-, K^+) reaction, the Ξ^- stopping in matter, and its atomic cascade are incorporated within a realistic evaluation of the results expected for Ξ^- X-ray spectra across the periodic table, using an assumed Ξ-nucleus optical potential V_{opt}. Several optimal targets for measuring the strong-interaction shift and width of the X-ray transition to the 'last' atomic level observed are singled out: F, Cl, I, Pb. The sensitivity of these observables to the parameters of V_{opt} is considered. The relevance of such experiments is discussed in the context of strangeness -2 nuclear physics and multistrange nuclear matter. Finally, with particular reference to searches for the H dibaryon, the properties of $\Xi^- d$ atoms are also discussed. The role of Stark mixing, its effect on S and P state capture of Ξ^- by the deuteron, together with estimates of the resulting probability for producing the H dibaryon are considered in detail.

PACS: 15.20.Jn, 36.10.Gv

February 9, 2008

I. INTRODUCTION AND BACKGROUND

Very little is established experimentally or phenomenologically on the interaction of Ξ hyperons with nuclei. Dover and Gal [1], analyzing old emulsion data which had been interpreted as due to Ξ^- hypernuclei, obtained an attractive Ξ-nucleus interaction with a nuclear potential well depth of $V_0^{(\Xi)} = 21 - 24$ MeV. This range of values agrees well with the theoretical prediction by the same authors [2] for Ξ in nuclear matter, using model D of the Nijmegen group [3] to describe baryon-baryon interactions in an SU(3) picture, in contrast with the Ξ-nucleus repulsion obtained [2] using model F [4]. Similar predictions were subsequently made with more detailed G matrix evaluations by Yamamoto *et al.* [5,6] who argued for a considerable A dependence of $V_0^{(\Xi)}$, such that the well depth for light and medium weight nuclei is significantly lower than for heavy nuclei where it approaches the value calculated for nuclear matter. It should be noted, however, that the predictions of the Nijmegen model D for $V_0^{(\Xi)}$ are extremely sensitive to the value assumed for the hard-core radius. Nevertheless, the confidence in the predictive power of model D for this sector of strangeness -2 hypernuclear physics, at least qualitatively, is to a large extent due to its success in yielding the attractive $\Lambda\Lambda$ interaction necessary to reproduce the (so far) three known $\Lambda\Lambda$ binding energies (see Ref. [5] for a review of these calculations).

If the interaction of Ξ hyperons with nuclei is sufficiently attractive to cause binding, as has been repeatedly argued since the original work of Dover and Gal [1], then a rich source of spectroscopic information becomes available and the properties of the in-medium ΞN interaction can be extracted. Bound states of Ξ hypernuclei would also be useful as a gateway to form double Λ hypernuclei [7,8]. Finally, a minimum strength for $V_0^{(\Xi)}$ of about 15 MeV is required to realize the exciting possibility of strange hadronic matter [9]; where protons, neutrons, Λs and Ξs are held together to form a system which is stable against strong-interaction decay.

Some new information on the Ξ^- nucleus interaction has been recently reported from $(K^-,\ K^+)$ counter experiments at the KEK proton synchrotron. Fukuda *et al.* [10] have shown fits to the very low energy part (including the bound state region) of the Ξ^- hypernuclear spectrum in the $^{12}\mathrm{C}(K^-, K^+)X$ reaction on a scintillating fiber active target (experiment E224), resulting in an estimate of $V_0^{(\Xi)}$ between 15 to 20 MeV. The experimental energy resolution of about 10 MeV in this experiment was too poor to allow identification of any bound state peak structure which could have given more definitive information on the well depth. A somewhat cleaner and better resolved spectrum has been recently shown [11] from the Brookhaven AGS experiment E885, but no analysis of these data has yet been reported. An earlier KEK experiment (E176) gave evidence for three events of stopped Ξ^- in light emulsion nuclei, each showing a decay into a pair of single Λ hypernuclei. The first two events [12,13] are consistent energetically with a Ξ^- *atomic* state in ^{12}C bound by $B_{\Xi^-}(^{12}\mathrm{C}) = 0.58 \pm 0.14$ MeV. However, this value could only be ascribed to capture from the $1S$ state which is estimated to occur in less than 1% of the total number of captures. This binding energy is distinctly larger than the calculated value $B_{\Xi^-}^{2P}(^{12}\mathrm{C}) \lesssim 0.32$ MeV for the $2P$ state, for a wide range of strong-interaction potentials. Moreover, the Ξ^- capture probability in ^{12}C from P states is a few percent at most. The most likely capture in ^{12}C, as discussed in Sec. III B, occurs from atomic D states. The calculated binding energies of the atomic $3D$ states for C, N, O emulsion nuclei are given in Table I where it is seen

that binding is essentially by the Coulomb potential. The two examples for binding in the presence of a strong Ξ-nucleus potential are for the $t\rho$ potential used in Sec. II and III with the parameter $b_0 = 0.25 + i0.04$ fm (potential 1) and $b_0 = 0.19 + i0.04$ fm (potential 2), corresponding to $V_0^{(\Xi)}$ =20.5 and 15.6 MeV, respectively, in ^{12}C. (The value used for Imb_0 is discussed in Sec. III A and IV). It is seen that the sensitivity of the binding energies and strong interaction widths to the Ξ-nucleus strong interaction is, for these examples, of the order of 100 eV, substantially smaller than a typical error of 100 keV incurred in emulsion work. We point out that there exist alternative interpretations of these two events as captures on ^{14}N, with binding energies consistent with the calculated value listed in the table, for example [12], $B_{\Xi^-}(^{14}\mathrm{N}) = 0.35 \pm 0.20$ MeV. Furthermore, a likely interpretation of the third event [14] is due to capture on ^{16}O, with $B_{\Xi^-}(^{16}\mathrm{O}) = 0.31 \pm 0.23$ MeV. Clearly, whereas these emulsion events are consistent with capture from $3D$ *atomic* states, they are useless as a source of information regarding the Ξ-nucleus interaction.

One clearly needs an alternative source of information on the Ξ-nucleus strong interaction. Such an alternative source is the measurement of X-ray energies from transitions between low lying levels of Ξ^- hadronic atoms. The experimental accuracies of the proposed measurements are such that meaningful information on the Ξ-nucleus interaction is likely to be obtained. In arguing the case for doing experiments with Ξ^- atoms, we follow the example of Σ^- atoms which, as was recently shown [15], gives rise to meaningful information about the Σ nucleus interaction, particularly in the absence of any systematic evidence for bound Σ hypernuclei.

Experiments with stopped Ξ^- hyperons had been proposed by Zhu *et al.* [16] and by Akaishi and collaborators [17] in order to produce some of the lightest ΛΛ hypernuclei, ${}^{6}_{\Lambda\Lambda}$He and ${}^{4}_{\Lambda\Lambda}$H (if the latter is particle stable) respectively, by looking for a peak in the outgoing neutron spectrum in the two-body reaction

$$\Xi^- \quad + \quad {}^{A}Z \quad \longrightarrow \quad {}^{A}_{\Lambda\Lambda}(Z-1) \quad + \quad n \quad . \tag{1}$$

These proposals motivated the AGS experiment E885 [11] on ^{12}C, using a diamond target to stop the Ξ^- hyperons resulting from the quasi-free peak of the (K^-, K^+) initial reaction. Finally, stopping Ξ^- hyperons in deuterium has been used in the AGS experiment E813 to search for the doubly strange H dibaryon through the reaction $(\Xi^- d)_{atom} \to Hn$, as reviewed recently by Chrien [18].

In Sec. II we consider the experimental features of measuring X-ray transitions in Ξ^- atoms, and in Sec. III we discuss possible target nuclei, using a $t\rho$ optical potential. Alternative choices, using density dependent optical potentials, are discussed in Sec. IV. The special case of Ξ^- atoms of deuterium, which is connected to recent searches for the H dibaryon, is discussed in Sec. V. Section VI summarizes the present work.

II. EXPERIMENTAL CONSIDERATIONS

In considering the feasibility of measuring strong interaction effects in Ξ^- atoms, we are guided by the successful observation and measurement of strong interaction effects [19–21] in Σ^- atoms. The Ξ^- and the Σ^- hyperons have very similar masses and lifetimes, namely 1321.32 and 1197.34 MeV for Ξ^- and Σ^- respectively, and 0.1642 and 0.1482 nsec for Ξ^- and

Σ^- respectively. Consequently, major differences between the experimental X-ray counting rates should result mostly from differences between the production mechanism of the two kinds of hadronic atoms. In the Σ^- case the production mechanism is the $K^-p \longrightarrow \Sigma^-\pi^+$ reaction at rest. The outgoing Σ^- has a kinetic energy of 12.4 MeV which means that it stops in a heavy target such as Pb or W in less than 10^{-11} sec and the outgoing pion has a kinetic energy of 83.2 MeV which makes it quite easy to detect. For the Ξ^- particle the situation is less favourable. The production mechanism is the $K^-p \longrightarrow \Xi^-K^+$ reaction which has a total cross section larger than 100 μb only in the kinetic energy range for K^- of 1.0 to 1.8 GeV (see results summarized in Ref. [1]). Consequently the majority of the produced Ξ^- will be in the energy range of 100 to 300 MeV, leading to stopping times in heavy targets of 0.01 to 0.3 nsec respectively. It is therefore essential that the Ξ^- particles slow down in a heavy degrader and not in the liquid hydrogen used for the production where the stopping times are much longer. A laminar target structure similar to that used in Σ^- experiments [21,22] seems the most suitable. Without detailed calculations for specific target and degrader configurations it is only possible to estimate that up to 50% of the produced Ξ^- may survive the slowing down process. Detection in coincidence with the outgoing K^+ is a must in such an experiment. The energy of this K^+ will be about 500 MeV.

When interested in the measurement of strong interaction effects in hadronic atoms it is also necessary to consider losses during the atomic cascade process. Here, again, it is possible to make use of the fact that Σ^- atoms have been successfully observed, and that the Ξ^- and the Σ^- hyperons have very similar masses and lifetimes. We have performed calculations of the atomic cascade for Σ^- atoms of Pb, in order to compare the predicted absolute X-ray yields with experiment [21].

The cascade program used here was based on that originally written by Hüfner [23] for muonic atoms and later modified to include strong interaction effects. The hadronic atom is assumed to be formed in a state of large radial quantum number n. To accommodate departures from a purely statistical distribution the initial population used is of the form

$$p(l) = (2l+1)e^{\alpha l} \tag{2}$$

where for $\alpha = 0$ the statistical distribution is obtained. The atom initially de-excites by Auger transitions and later by radiative transitions with the emission of X-rays. Finally in a state of low angular momentum l the hadron is absorbed by the nucleus and the X-ray cascade terminates. The probabilities for Auger and radiative transitions are calculated with the usual electromagnetic expressions [24]. For the strong interaction the input to the calculations are the measured or calculated absorption widths of low n circular $(n, l = n-1)$ atomic states which are then scaled [25] to obtain widths for non-circular states of a given l and increasing n. The probability that the hadron may decay during the atomic cascade is also included in the calculation.

For the strong interaction widths we used values predicted by the density dependent Σ nucleus potential which reproduces all the available data [15]. From a fit to the measured relative X-ray yields [21] we obtain the value $\alpha = -0.056 \pm 0.020$ which corresponds to a small departure from a purely statistical distribution. The predicted absolute yields for the three transitions of interest are shown in Fig. 1 where it is seen that their variation with α over its fitted range of uncertainty is not very large. Note that the $11M \rightarrow 10L$ and $10L \rightarrow 9K$ transitions in Σ^- Pb have been observed [21]. Next we calculated the yields for

Ξ^- atoms of Pb for a range of values of α. Strong interaction widths of the relevant levels were calculated with a $t\rho$ potential with $b_0 = 0.25 + i0.04$ fm as discussed below. Figure 2 shows the calculated absolute yields, which turn out to be very similar to the corresponding values for the Σ^- Pb atom. In both cases the $13 \rightarrow 11$ transition is also shown because its energy is very close to that of the $10 \rightarrow 9$ transition and the two will have to be separated. It is therefore concluded that Ξ^- atoms could be observed if the production yield and detection efficiency are not too small compared to the corresponding values for Σ^- atoms.

III. SELECTION OF TARGETS

A. Potentials and criteria

When selecting targets for possible experiments on Ξ^- atoms, it must be assumed that such experiments will probably not be feasible on more than very few targets, and one must therefore ask whether it is at all likely that useful information on the interaction of Ξ^- with nuclei will be obtained from the resulting rather limited range of data. Useful hadronic-atom data normally consist of the strong-interaction shift and width for the 'last' level observed plus, occasionally, the relative yield for the 'upper' level, as discussed below. It has been shown very recently [26] that the main features of the interaction of K^- and Σ^- with nuclei, as found from analyses of all the available data, may in fact, be obtained by analyzing a small fraction of the available hadronic atom data, if the target nuclei are carefully selected. A key point here is to have target nuclei over as wide a range of the periodic table as possible. This observation suggests that experiments on Ξ^- atoms may provide useful information.

In order to have some idea of the expected strong interaction effects in Ξ^- atoms and on the expected yields of X-ray transitions, it is necessary to adopt some form of an optical potential which will describe, at least approximately, the interaction of the Ξ^- hyperon with nuclei and its dependence on the nuclear mass. The so-called $t\rho$ potential [27] in its simplest form is given by

$$2\mu V_{opt}(r) = -4\pi(1 + \frac{\mu}{M})b_0\rho(r) \tag{3}$$

where μ is the Ξ-nucleus reduced mass, M is the mass of the nucleon and $\rho(r)$ is the nuclear density, normalized to the mass number A. The parameter b_0 is a complex parameter, and is usually related to the hadron-nucleon scattering length [27]. More refined potentials have been used with other hadronic atoms and will be discussed in the following section. For the present purpose we select the value of $\mathrm{Re}b_0 = 0.25$ fm which yields a potential depth of about 20 MeV inside nuclei, and $\mathrm{Im}b_0 = 0.04$ fm, yielding for the imaginary potential a depth of about 3 MeV. Whereas the real potential may be regarded as 'typical', according to the discussion in Sec. I, the imaginary potential is about twice as large as estimated [5] in model D. Reducing the imaginary potential will only cause the calculated widths of the states to decrease by roughly the same proportion, and the relative yields (see below) of transitions to become larger. This will not, however, change the last observed atomic level. A further comment on the choice of the imaginary potential is made in Sec. IV.

In choosing criteria for the suitability of a transition as a source of information on the Ξ nucleus interaction, we are guided by experience with other hadronic atoms [27,28] and

select X-ray transitions $(n+1, l+1) \rightarrow (n, l)$ between circular atomic states $(n = l + 1)$ with energies greater than 100 keV, where the strong interaction shift for the 'last' (n, l) level is at least 0.5 keV and the width less than about 10 keV. The 'upper' level relative yield, defined as the ratio of the intensity of the $(n+1, l+1) \rightarrow (n, l)$ X-ray transition to the summed intensity of all X-ray transitions feeding the $(n+1, l+1)$ state, is also required to be at least 10%. The 'upper' level relative yield [28] is given by the ratio of the radiative width for the $(n+1, l+1) \rightarrow (n, l)$ transition to the total width of the $(n+1, l+1)$ level feeding the (n, l) level. A measurement of the relative yield enables the strong interaction width of the 'upper' $(n+1, l+1)$ level to be determined, in addition to deducing the strong-interaction level shift and width for the 'last' (n, l) level from the X-ray transition energy discussed above. Altogether, these are the strong-interaction data provided by measuring atomic X-ray spectra.

B. Results

Strong interaction shifts and widths of Ξ^- atomic levels have been calculated using the above optical potential for a large number of nuclei. As the overlap of atomic wavefunctions with nuclei vary smoothly with charge number, it is to be expected that generally shifts, widths and yields will vary smoothly along the periodic table. Figure 3 shows calculated widths and 'upper' level relative yields for the $9K$ level in Ξ^- atoms for several heavy targets. Calculated shifts (not shown) for the chosen potential are generally equal to or up to 30% larger than the widths, as long as both are smaller than 10 keV. It is seen from the figure that Pb is a suitable target for the experiment. Figure 4 shows similar results for the $7I$ state in medium-heavy Ξ^- atoms and it is seen that a suitable target may be found near Sn or I. The dashed lines in this figure are obtained by reversing the sign of the real potential used for calculating the solid curves. It is seen that in such a case the range of suitable targets will move to between I and Ba, where the strong interaction width and relative yield are more acceptable. The sign of the strong interaction shift will be reversed in this case, but it has no experimental consequences. This exemplifies a general property of hadronic atoms, which are dominated by the Coulomb interaction, namely, that large variations in the strong interaction potential will move the proposed targets only a few units of charge along the periodic table.

Figure 5 shows results for the $4F$ state of Ξ^- atoms, where it is seen that for a Si target the effects could be too small to measure whereas for Ca the width could be too large and the relative yield too small. In this region a Cl target may be appropriate, perhaps in the form of the liquid CCl_4. More detailed results for Cl are shown in Fig. 6 where the sensitivities to assumptions regarding the optical potential are also typical of results for other targets. The solid curves connect points obtained within the $t\rho$ potential Eq. (3) for fixed values of $\mathrm{Re}b_0$, listed above the lines. The four points along each line correspond to values of $\mathrm{Im}b_0$ from 0.05 fm down to 0.02 fm in steps of 0.01 fm. Departures from this $t\rho$ potential are represented by the dotted lines, calculated from phenomenological density dependent (DD) real potentials similar to those found from analyses of experimental results for Σ^- and K^- atoms [27]. The imaginary part of the potential is of the $t\rho$ type and the points along the dotted lines correspond to the same values of $\mathrm{Im}b_0$ as above. The real potentials in these calculations are similar to the real potential for Σ^- atoms [27], having an attractive pocket

about 5-10 MeV deep outside the nuclear surface, with a repulsive potential of about 20-30 MeV in the nuclear interior. The results in the figure serve only to illustrate the expected range of strong interaction effects. If the actual values of shift and width turn out to be within the area covered by the lines, these effects will most likely be measurable.

Figure 7 shows calculated results for $3D$ states in several Ξ^- atoms, and it is seen that F may be a suitable target, possibly in the form of teflon (CF_2). To see what could be the effects of the carbon in the target we have also performed full atomic cascade calculations for C and F, and the expected X-ray spectrum for teflon is shown in Fig. 8. It seems that the presence of carbon in the target should not affect the possibility of observing transitions in Ξ^- F atoms.

Results for the $t\rho$ potential with $b_0 = 0.25 + i0.04$ fm are summarized in Table II, which includes several suitable targets across the periodic table where strong interaction effects are likely to be measurable. A range of targets is necessary if unusual features of the interaction, such as density dependence beyond the $t\rho$ prescription, are to be unraveled by the experiment.

IV. Ξ NUCLEUS DENSITY DEPENDENT POTENTIALS

In the previous section we have discussed Ξ^- X-ray spectra across the periodic table, assuming a Ξ-nucleus strong interaction potential of the form $V^{(\Xi)} = t\rho$, Eq. (3). Specific predictions were given, using the value $b_0 = 0.25 + i0.04$ fm, and the sensitivity to departures from this value was displayed in Fig. 4 and 6. Conversely, one may explore the extent to which measuring, say, four X-ray spectra (e.g. Table II) will determine the Ξ-nucleus potential. In the present section we address this question by choosing a one-boson-exchange (OBE) motivated Ξ-nucleus potential, use it to evaluate the strong-interaction shifts and widths for several targets across the periodic table, and then solve the inverse problem, namely determine the best-fit parameters for Ξ nucleus potentials of different forms.

We start with the ΞN DD G-matrix interaction YNG derived by Yamamoto *et al.* [5] from the Nijmegen OBE potential model D [3]:

$$v_{\Xi N}\left(r;k_F\right) = \sum_{i=1}^{3}\left(a_i + b_i k_F + c_i k_F^2\right)\exp\left(-r^2\big/\beta_i^2\right) , \tag{4}$$

where the nuclear Fermi momentum k_F is expressed in terms of the local nuclear density ρ, $k_F = \left(3\pi^2\rho/2\right)^{1/3}$. To simplify matters, while retaining a substantial part of the density dependence of $v_{\Xi N}$, we kept only the a and b terms. These G-matrix parameters are listed in Table III for the choice $r_c = 0.46$ fm, which belongs to the range of values considered in Ref. [5]. We note that the G matrix depends strongly on the hard-core radius r_c chosen in the ΞN sector of model D. The resulting $v_{\Xi N}$ is repulsive at short ΞN distances and attractive at distances $r \geq 0.8$ fm. The Ξ nucleus DD real potential, obtained by folding $v_{\Xi N}$ with the nuclear density ρ:

$$V^{(\Xi)}\left(r;\rho\right) = \int v_{\Xi N}\left(\left|\mathbf{r}-\mathbf{r}'\right|;k_F\left(\rho\right)\right)\rho\left(r'\right)d^3r' , \tag{5}$$

is shown in Fig. 9 (G, solid line) for the nucleus Sn. Its depth is about 18 MeV (attractive) in medium-weight and heavy nuclei and about half of that in light nuclei, so it falls conveniently

within the range of values considered as 'realistic' in Sec. I. However, as is clear by comparing the shape of this $V^{(\Xi)}$ (potential G) with the (fitted, see below) $t\rho$ potential, plotted as a dot-dash line in the figure, potential G extends considerably further out than does the nuclear density distribution ρ . The difference in the r.m.s. radius values amounts to about 1.3 fm. The main contribution to this difference does not arise just from folding the finite-size $v_{\Xi N}$ into ρ, but is due to the summed effect of the DD terms 'b' which produce repulsion on top of the attractive contribution due to the sum of the 'a' terms. Retaining the 'c' terms in Eq. (4) would have reduced the r.m.s. radius of potential G, but in addition it would have increased the nuclear-matter depth to about 30 MeV, a value which currently [10] is considered to be a gross overestimate.

For the imaginary part of $V^{(\Xi)}$ we retained, for simplicitly, the $t\rho$ form with $\mathrm{Im}b_0 = 0.04$ fm as before. We checked that replacing it by the corresponding DD form [5], as per Eqs. (4,5), has a marginal effect on our results. The reason is that since the real part of $V^{(\Xi)}$ is substantially stronger than the imaginary part, the main effect of the density dependence is due to the real part of $V^{(\Xi)}$.

The calculated strong-interaction shifts and widths, using potential G, are shown in Table IV for several target nuclei, including the five targets listed in Table II which were motivated by the $t\rho$ potential with a similar depth. Where comparison can be made, these shifts and widths are larger by an order of magnitude than those in Table II, due to the greater extension of potential G which pulls in the atomic wavefunctions by up to 2 fm (judging by the inward shift of the position of the maximum of the atomic wavefunctions at about 20 fm). Consequently, with most of the calculated shifts and widths exceeding 10 keV, the targets (F, Cl, I, Pb) will no longer be the optimal ones for experiments with Ξ^- atoms. As discussed in Sec. III B, one can identify neighbouring targets by going several charge units down in each sequence to reestablish optimum conditions. Indeed, according to Table IV, an optimal set of targets could consist of (O, S, Sn, W).

For testing the inversion procedure under the extreme conditions set up by using potential G, the shifts and widths calculated for these four Ξ^- atoms were considered as pseudo data. Standard measurement errors of 20% were ascribed, and randomized values of these pseudo data quantities were then derived and used for fitting a given form of the real potential $V^{(\Xi)}$ (the imaginary part was always taken as $t\rho$). Two forms were used:

(i) The $t\rho$ form, but with b_0 determined from the fit. The best fit parameter b_0 was found to be

$$\mathrm{Re}b_0 = 0.402 \pm 0.022 \ \ \mathrm{fm}, \qquad \mathrm{Im}b_0 = 0.053 \pm 0.021 \ \ \mathrm{fm},$$

with χ^2/F, the χ^2 of the fit per degree of freedom, assuming a relatively high value of $\chi^2/F = 8.8$. The real part of this potential is shown in Fig. 9. Note that it is twice as deep in the nuclear interior as potential G, owing to the analytic continuation from the surface region where the *fitted* potential must assume larger values than before. However, with such a distinct difference between the geometries of the two potentials, the quality of fit produced by the $t\rho$ best-fit potential to the pseudo data due to potential G is rather poor.

(ii) A phenomenological DD potential of the form Eq. (3), where the parameter b_0 now depends on density:

$$b_0(\rho) = b_0 + B_0[\rho(r)/\rho(0)]^\alpha. \tag{6}$$

For the imaginary part, the $t\rho$ form Eq. (3) was maintained, i.e. Im$B_0 = 0$. If the exponent α is taken as $\alpha = 1/3$, in order to simulate the density dependence of the underlying G-matrix $v_{\Xi N}$ (Eq. (4)), then the best-fit parameters are

$$\begin{aligned} \mathrm{Re}b_0 &= 1.27 \pm 0.21 \ \ \mathrm{fm}, \qquad \mathrm{Im}b_0 = 0.019 \pm 0.009 \ \ \mathrm{fm}, \\ \mathrm{Re}B_0 &= -1.05 \pm 0.26 \ \ \mathrm{fm}, \qquad \chi^2/F = 4.65. \end{aligned}$$

This potential is similar in depth to potential G, its r.m.s. radius is substantially larger than that of the $t\rho$ potential, and as $\rho \to 0$ it is about 3 times stronger than the best-fit $t\rho$ potential discussed above. The quality of this fit is quite reasonable.

If α is allowed to vary, it is found that the value $\alpha = -0.7$ provides a very good fit to the pseudo data:

$$\begin{aligned} \mathrm{Re}b_0 &= 0.268 \pm 0.033 \ \ \mathrm{fm}, \qquad \mathrm{Im}b_0 = 0.040 \pm 0.009 \ \ \mathrm{fm}, \\ \mathrm{Re}B_0 &= 0.056 \pm 0.011 \ \ \mathrm{fm}, \qquad \chi^2/F = 1.77. \end{aligned}$$

This best-fit phenomenological DD potential is also plotted in Fig. 9. It is deeper within the nucleus than potential G, becoming less attractive than the latter in the immediate surface region outside the nucleus, and then (since α is negative) becoming more attractive in the more extreme surface region (8 fm and beyond, for Sn).

It is clear that neither the oversimplified $t\rho$ potential, nor the phenomenological DD potentials defined by Eq. (6), are capable of reproducing the oscillatory behaviour of potential G in the nuclear surface region. The best-fit phenomenological DD potential probably gives a reliable indication of the overall attractive nature of the underlying potential $V^{(\Xi)}$, both yielding similar strengths of about 10 MeV in the nuclear surface region. It is noteworthy that the fitted imaginary part is practically the same for both potentials, probably due to the same $t\rho$ form assumed in the two cases.

V. Ξ^- DEUTERIUM ATOMS

In the previous sections we have discussed the possible observation of X-rays from Ξ^- atoms formed in nuclear targets and the possibility of obtaining information about strong interaction effects in Ξ^- atoms. In the present section we discuss the properties of $\Xi^- d$ atoms and in particular the formation of the doubly strange H dibaryon through the reaction $(\Xi^- d)_{atom} \to Hn$. An experiment to search for this reaction is in progress [29]. The formation of the H particle is detected by observation of the monoenergetic neutron, whilst the Ξ^- is tagged by the observation of the K^+ from the production reaction $K^- p \longrightarrow \Xi^- K^+$ as discussed earlier in Sec. II. The probability for H dibaryon formation from $\Xi^- d$ atoms has been calculated by Aerts and Dover [30] for reactions involving S and P states of the $\Xi^- d$ atom as a function of the mass of the H particle. (See Table II and Fig. 4 of Ref. [30]). Here we are specifically concerned with calculating the probability for the Ξ^- to interact with the deuteron from an atomic S or P state in the $\Xi^- d$ atom.

For the $\Xi^- d$ atom, the atomic cascade proceeds generally as described in Sec. II but with an additional complication due to the presence of Stark mixing [31]. This gives rise to transitions of the type $(n, l \pm 1) \leftrightarrow (n, l)$ which increases the probability of $\Xi^- d$ interactions

from atomic S states at large values of n. Since the Stark mixing is proportional to the collision rate, and hence target density, the effects are largest in liquid hydrogen. As the interactions take place at high n, the lifetime of the $\Xi^- d$ atom is reduced by the Stark mixing and the probability for the Ξ^- to decay during the atomic cascade decreases.

Some of the early qualitative discussions of Stark mixing [31] for $K^- p$ atoms were placed on a more quantitative basis by Leon and Bethe [32]. Their calculations were later modified and extended by Borie and Leon [33] to a range of exotic-hydrogen atoms such as $\mu^- p$, $\pi^- p$, $K^- p$ and $\bar{p}p$. Of interest for the present work, calculations using the Borie and Leon model have been used to fit measured X-ray yields for K- and L-series X-rays from antiprotonic hydrogen ($\bar{p}p$) atoms [34]. In using this model it has generally been found that, because of approximations in the calculation of the absolute value of the Stark mixing rate, an overall normalisation factor k_{STK} is required to get a good fit to the experimental X-ray data. Typical values of k_{STK} required to fit data for $\bar{p}p$ atoms are in the range 1.0 to 2.0. In the present work calculations are made for k_{STK} over the range 0.5 to 5.0.

The present calculations were carried out using the Borie and Leon model [33] with the program used in [34] for calculations on antiprotonic hydrogen atoms, modified for $\Xi^- d$ atoms and including decays of the Ξ^-. The principal input values are the Stark mixing normalization factor k_{STK} and the strong interaction widths Γ_{1S} and Γ_{2P} for the $1S$ and $2P$ levels respectively. The strong interaction width of the $3D$ and higher $(n, l = n-1)$-states were all set to zero. The kinetic energy of the $\Xi^- d$ atom was taken to be 1 eV [33].

The total strong interaction widths calculated by Aerts and Dover [30] lie in the range $\Gamma_{1S} = 1$ to 50 keV for S states and $\Gamma_{2P} = 0.2$ to 0.8 eV for P states. In Fig. 10 the fraction of S and P state reactions as a function of the Stark mixing parameter k_{STK} is shown for three sets of strong interaction parameters, $\Gamma_{1S} = 10$ keV, $\Gamma_{2P} = 0.2$ eV (labelled 1), $\Gamma_{1S} = 10$ keV, $\Gamma_{2P} = 0.8$ eV (labelled 2) and $\Gamma_{1S} = 1$ keV, $\Gamma_{2P} = 0.2$ eV (labelled 3). The fraction of $\Xi^- d$ atoms which decay is also plotted for case 1; cases 2 and 3 give almost indistinguishable values. The results are seen to exhibit only small sensitivity to the choice of strong interaction parameters, but considerable sensitivity to the value of k_{STK}. As the amount of Stark mixing increases, the fraction of S state capture increases, P state capture decreases and the number of Ξ^- decays from the $\Xi^- d$ atom is reduced as expected.

A particular feature of the Borie and Leon model is that it seems to over-estimate the amount of P state capture. This problem has been discussed by Batty [35] for $\bar{p}p$ atoms. He finds that the introduction of an additional normalization factor K_0, used for Stark transitions between S and P states only, *i.e.* $nS \rightarrow nP$ and $nP \rightarrow nS$ transitions, gives significantly improved fits to the X-ray yield data with $K_0 = 7.6$ and much reduced values for the fraction of P state annihilation in liquid hydrogen.

Here we use the same model and again fix $K_0 = 7.6$. There is no particular reason for this choice of value for K_0 except that it gives a good fit to the $\bar{p}p$ atom results. The resulting values for the fraction of S and P state capture and of Ξ^- decays are plotted in Fig. 11 for the same values of the strong interaction parameters as used in Fig. 10 which is equivalent to the case with $K_0 = 1.0$. Setting $K_0 = 7.6$ as in Fig. 11 decreases the P state fraction and increases the S state fraction, as is to be expected for the increased amount of Stark mixing between S and P states and as was also shown by the $\bar{p}p$ calculations. The results now show slightly more sensitivity to the strong interaction parameters Γ_{1S} and Γ_{2P}. However the fraction of Ξ^- decays largely stays unaltered.

Using S and P state capture fractions obtained in this way, with values for Γ_{1S} and Γ_{2P} given in Table II of Ref. [30], the probability for the production of the H particle from $\Xi^- d$ atoms can be calculated [36]. Aerts and Dover [30] also give in Fig. 4 of their paper, values, as a function of the mass of the H particle m_H, for the branching ratios R_S and R_P defined by,

$$R_S = \Gamma((\Xi^- d)_{1S} \rightarrow Hn)/\Gamma_{1S} \tag{7}$$

and

$$R_P = \Gamma((\Xi^- d)_{2P} \rightarrow Hn)/\Gamma_{2P}. \tag{8}$$

Weighting the fractions of S and P state capture by the corresponding R_S and R_P (values for model D in Ref. [30] were used), then gives the total probability for H particle production as a function of the binding energy $B(H)$. Here $B(H)$ is the binding energy of the H particle relative to the $\Lambda\Lambda$ mass. The results are shown in Fig. 12 for four different values of k_{STK} = 0.5, 1.0, 2.0 and 5.0 (curves labelled 1, 2, 3, and 4 respectively) and for $K_0 = 1.0$ and 7.6 (dashed and solid lines respectively).

The results of [30] show that H particle production is more likely to proceed from S states rather than P states by a factor varying from 1.4 at $m_H = 2.23$ GeV ($B(H) = 0$ MeV) to 14 at $m_H = 2.18$ GeV ($B(H) = 50$ MeV). As a result the probability of H particle production increases with Stark mixing (increasing k_{STK} or K_0) as can be clearly seen from Fig. 12.

On the other hand the branching fractions R_S and R_P both decrease as the binding energy $B(H)$ increases. However the fraction of S state capture increases somewhat from 0.46 to 0.57 and the P state fraction decreases from 0.38 to 0.27 as $B(H)$ increases from 0 to 50 MeV. These changes are largely due to the reduction in the $2P$ state strong interaction width Γ_{2P} from 0.61 to 0.25 eV as $B(H)$ increases; the above capture fractions were calculated for $k_{STK} = 1.0$ and $K_0 = 7.6$. As a result, due to the increase in S state capture, the decrease in H particle production with increasing $B(H)$ is less rapid than might be deduced solely from the overall reduction in the branching fractions for H particle production from the $\Xi^- d$ atom.

VI. SUMMARY

Almost no quantitative information on the interaction of Ξ^- hyperons with nuclei is available at present and it is unlikely that conventional measurements of particle energies to investigate Ξ^- hypernuclei will have sufficient accuracy to alter this situation. In contrast, the usual precision for measuring the energies of X-rays from transitions between levels of hadronic atoms offers the possibility of obtaining quantitative information on the interaction of Ξ^- hyperons with nuclei. In the present work we have been guided by the successful observation and reasonably precise measurement of strong interaction effects in Σ^- atoms, which has led to our best knowledge, so far, of the interaction of Σ^- hyperons with nuclei.

Full atomic cascade calculations have been performed for Σ^- and Ξ^- atoms and confirmed, as expected, that the processes within these two hadronic atoms are very similar. The remaining major differences are in the production reactions. Whereas Σ^- hyperons are produced by the $p(K^-, \pi^+)\Sigma^-$ reaction at rest, the $p(K^-, K^+)\Xi^-$ reaction occurs at higher

energies, thus causing decay losses during the slowing down time of the Ξ^- particle to be non-negligible. Prior to such an experiment it will be necessary to optimize the experimental setup, which includes a hydrogen production target, a heavy moderator such as Pb or W, the target to be studied and the detectors, both for X-rays and for the detection of the outgoing K^+, which is essential in order to reduce background.

In the present work we have confined ourselves to studying the dependence of strong interaction shifts and widths in Ξ^- atoms on the various parameters of the problem, including the nuclear charge. Adopting an optical potential for the strong interaction between the Ξ^- and the nucleus and assuming it to be attractive and 15-20 MeV deep with an imaginary part of 1-3 MeV, we are able to propose four targets along the periodic table, namely, F, Cl, I and Pb as suitable for X-ray measurements. This also proves to be a sensible choice of targets for moderate changes in V_{opt}. Nevertheless, even if the actual potential turns out to be very different from the one used in the present calculations, for example using potential G of Sec. IV, only relatively small changes will result, because the whole phenomenon of hadronic atoms is dominated by the Coulomb interaction. Starting from a G-matrix based ΞN interaction, we constructed a version of $V^{(\Xi)}$ (potential G) which would indeed lead to a slightly different choice of optimal targets. It was shown that the qualitative features of such a potential can be deduced by an inversion procedure, where one fits a phenomenological DD potential to the strong interaction data deduced from Ξ^- atom experiments. Although we do not consider potential G as a realistic one, this example served to demonstrate the feasibility of the inversion procedure.

Finally, the special case of $\Xi^- d$ atoms has been discussed in great detail, in view of its role in current experiments aimed at the H dibaryon. The role of Stark mixing, its effect on S and P state capture of Ξ^- by the deuteron, together with estimates of the resulting probability for producing the H dibaryon have been considered in detail.

Some of the early calculations on $\Xi^- d$ atoms were carried out in collaboration with G. T. A. Squier. The estimates of H particle production from $\Xi^- d$ atoms were made by J. Lowe. This research was supported by THE ISRAEL SCIENCE FOUNDATION founded by The Academy of Sciences and Humanities.

REFERENCES

[1] C.B. Dover and A. Gal, Ann. Phys. (N.Y.) **146**, 309 (1983).
[2] C.B. Dover and A. Gal, Prog. Part. and Nucl. Phys. **12**, 171 (1984).
[3] M.M. Nagels, T.A. Rijken, and J.J. de Swart, Phys. Rev. D **15**, 2547 (1977).
[4] M.M. Nagels, T.A. Rijken, and J.J. de Swart, Phys. Rev. D **20**, 1633 (1979).
[5] Y. Yamamoto, T. Motoba, H. Himeno, K. Ikeda, and S. Nagata, Prog. Theor. Phys. Suppl. No. **117**, 361 (1994).
[6] Y. Yamamoto, in *Nuclear and Particle Physics with Meson Beams in the 1 GeV/c Region*, edited by S. Sugimoto and O. Hashimoto (Universal Academy Press, Inc. Tokyo, 1995), p. 267; Few-Body Syst. Suppl. **9**, 145 (1995).
[7] D.J. Millener, C.B. Dover, and A. Gal, Prog. Theor. Phys. Suppl. No. **117**, 307 (1994); C.B. Dover, A. Gal, and D.J. Millener, Nucl. Phys. **A572**, 85 (1994).
[8] K. Ikeda, T. Fukuda, T. Motoba, M. Takahashi, and Y. Yamamoto, Prog. Theor. Phys. **91**, 747 (1994); Y. Yamamoto, T. Motoba, T. Fukuda, M. Takahashi, and K. Ikeda, Prog. Theor. Phys. Suppl. No. **117**, 281 (1994).
[9] J. Schaffner, C.B. Dover, A. Gal, C. Greiner, and H. Stoecker, Phys. Rev. Lett. **71**, 1328 (1993); Ann. Phys. (N.Y.) **235**, 35 (1994); S. Balberg, A. Gal, and J. Schaffner, Prog. Theor. Phys. Suppl. No. **117**, 325 (1994).
[10] T. Fukuda *et al.*, Phys. Rev. C **58**, 1306 (1998).
[11] M. May, Nucl. Phys. **A639**, 363c (1998).
[12] S. Aoki *et al.*, Prog. Theor. Phys. **89**, 493 (1993).
[13] S. Aoki *et al.*, Phys. Lett. **B 355**, 45 (1995).
[14] K. Nakazawa, T. Sasaki, and Y. Yamamoto, in *Proceedings of the Workshop on Hypernuclear Physics*, edited by T. Motoba, Y. Akaishi, and T. Nagae [Genshikaku Kenkyu **41** No. **6**, 75 (1997)]; we are indebted to D.H. Davis for briefing us on this interpretation.
[15] C.J. Batty, E. Friedman, and A. Gal, Prog. Theor. Phys. Suppl. No. **117**, 227 (1994).
[16] D. Zhu, C.B. Dover, A. Gal, and M. May, Phys. Rev. Lett. **67**, 2268 (1991).
[17] I. Kumagai-Fuse, T. Koike, and Y. Akaishi, Nucl. Phys. **A585**, 367c (1995).
[18] R.E. Chrien, Nucl. Phys. **A629**, 388c (1998).
[19] G. Backenstoss, T. Bunaciu, J. Egger, H. Koch, A. Schwitter, and L. Tauscher, Z. Phys. **A273**, 137 (1975).
[20] C.J. Batty, S.F. Biagi, M. Blecher, S.D. Hoath, R.A.J. Riddle, B.L. Roberts, J.D. Davies, G.J. Pyle, G.T.A. Squier, and D.M. Asbury, Phys. Lett. **B 74**, 27 (1978).
[21] R.J. Powers *et al.*, Phys. Rev. C **47**, 1263 (1993).
[22] D.W. Hertzog *et al.*, Phys. Rev. D **37**, 1142 (1988).
[23] J. Hüfner, Z. Phys. **195**, 365 (1966).
[24] Y. Eisenberg and D. Kessler, Nuovo Cimento **19**, 1195 (1961).
[25] C.J. Batty and R.E. Welsh, Nucl. Phys. **A589**, 601 (1995).
[26] E. Friedman, Nucl. Phys. **A639**, 511c (1998).
[27] C.J. Batty, E. Friedman, and A. Gal, Phys. Rep. **287**, 385 (1997).
[28] C.J. Batty, Sov. Jour. Part. Nucl. **13**, 71 (1982).
[29] B. Bassalleck, in *Intersections between Particle and Nuclear Physics:* 6^{th} *Conference, Big Sky, MT May 1997*, edited by T.W. Donnelly, AIP Conference Proceedings **412**, 457 (New York, 1997); Nucl. Phys. **A639**, 401c (1998).
[30] A.T.M. Aerts and C.B. Dover, Phys. Rev. D **29**, 433 (1984).

[31] T.B. Day, G.A. Snow and T. Sucher, Phys. Rev. Lett. **3**, 61 (1959); Phys. Rev. **118**, 864 (1960).
[32] M. Leon and H.A. Bethe, Phys. Rev. **127**, 636 (1962).
[33] E. Borie and M. Leon, Phys. Rev. A **21**, 1460 (1980).
[34] C.J. Batty, Rep. Prog. Phys. **52**, 1165 (1989).
[35] C.J. Batty, Nucl. Phys. **A601**, 425 (1996).
[36] J. Lowe (private communication).

FIGURES

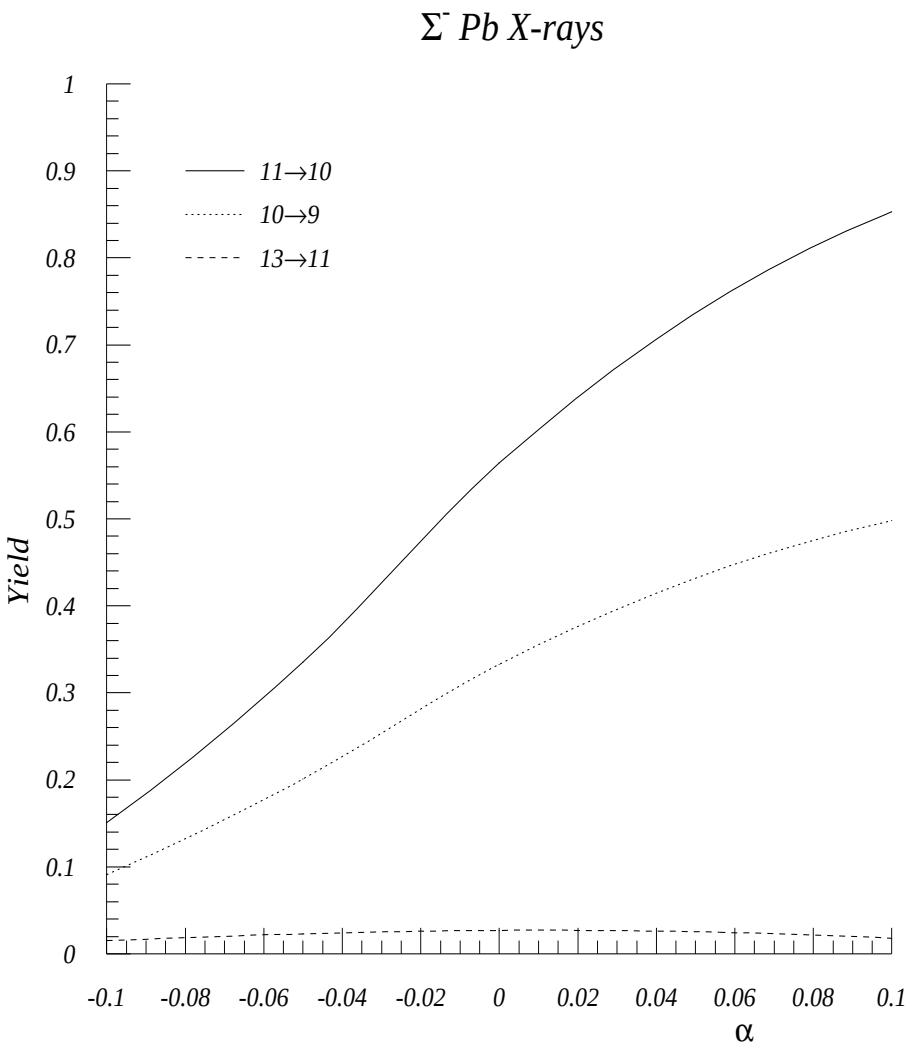

FIG. 1. Calculated absolute yields of X-ray transitions in Σ^- Pb atoms as a function of the initial population parameter α. Results are shown for $n_i \to n_f$ transitions with $l = n - 1$.

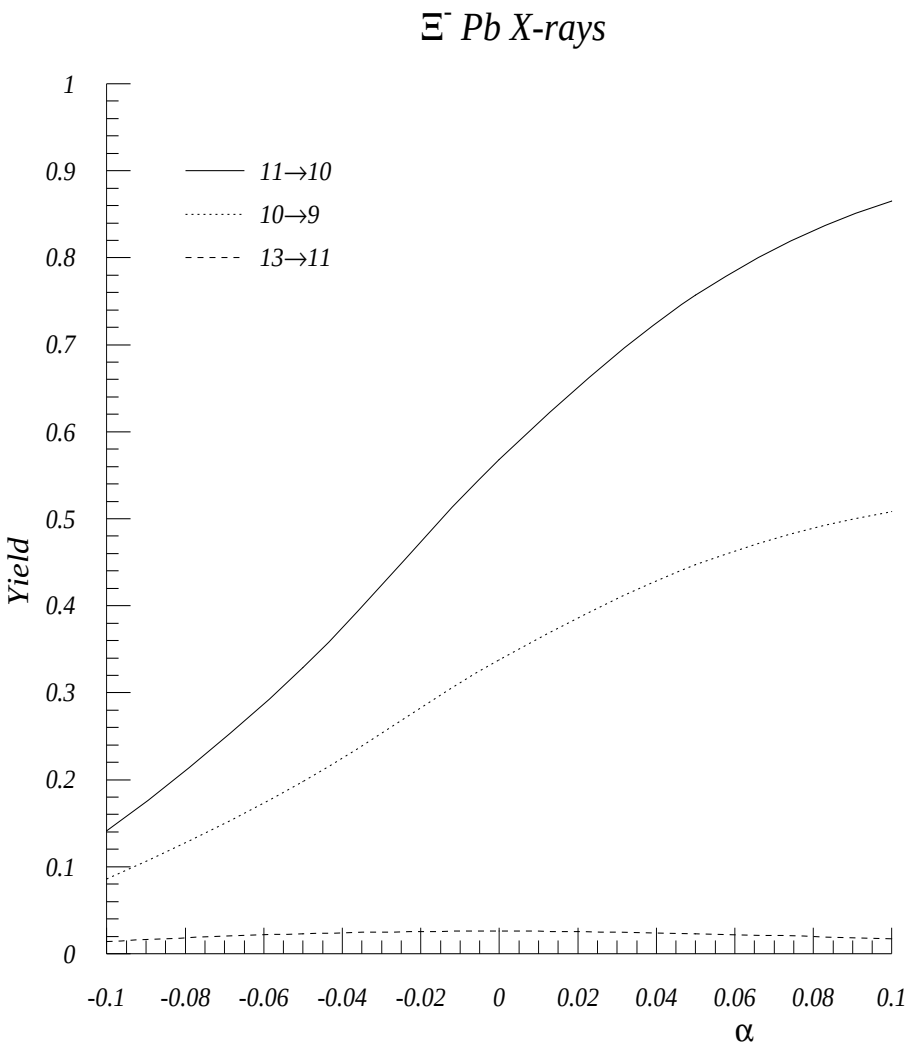

FIG. 2. Same as Fig. 1 but for Ξ^- Pb atoms.

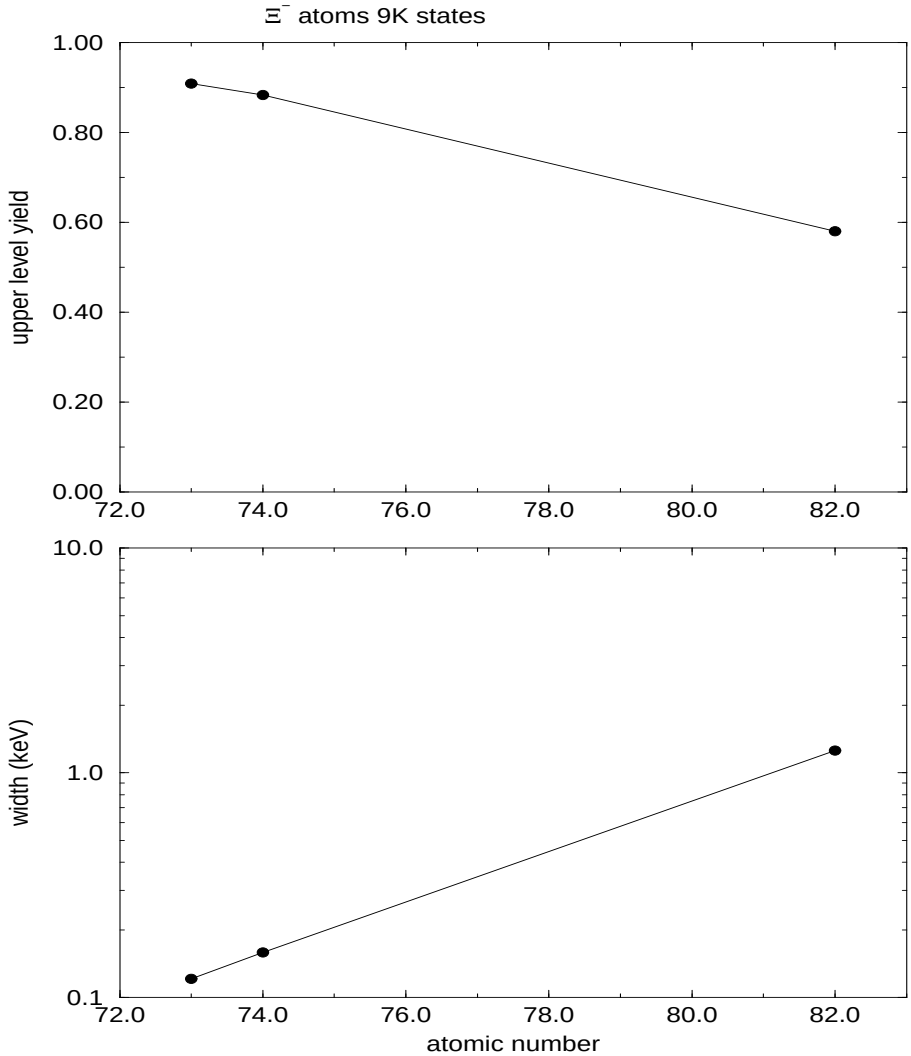

FIG. 3. Calculated strong interaction widths and upper level relative yields for the $9K$ level in heavy Ξ^- atoms.

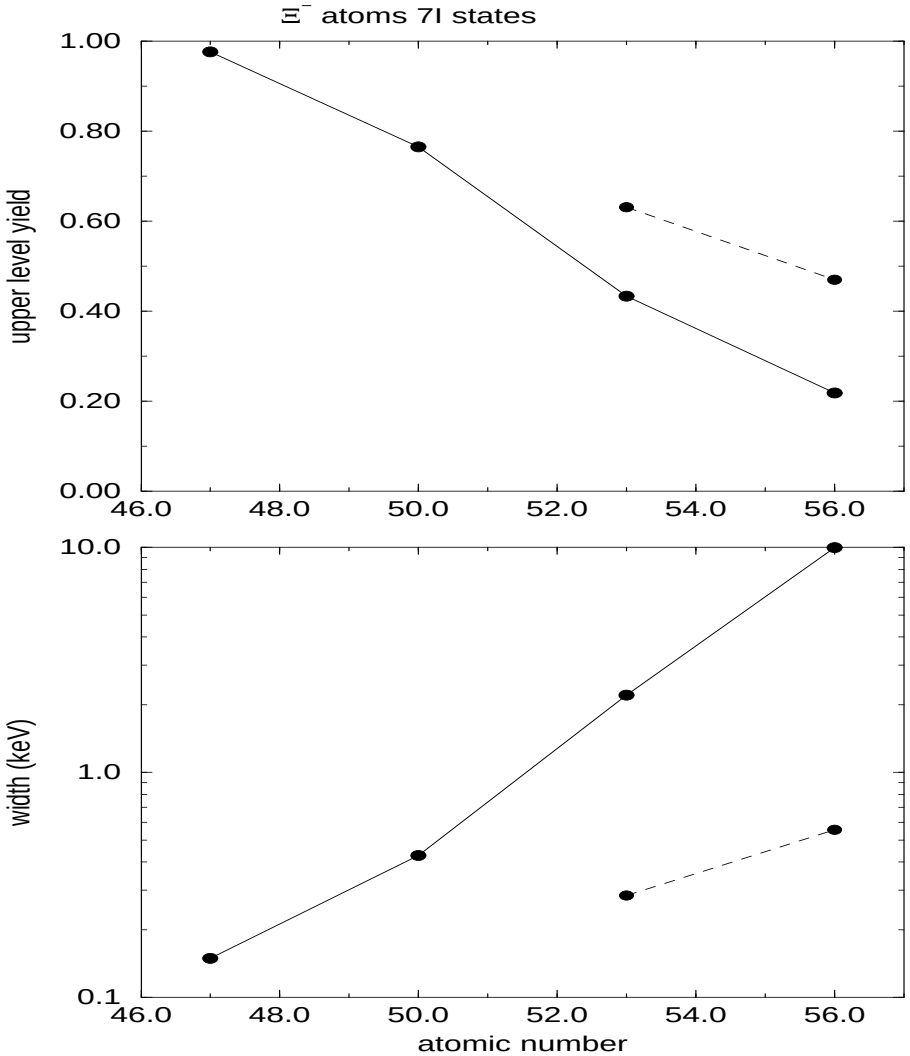

FIG. 4. Solid curves: calculated strong interaction widths and upper level relative yields for the $7I$ level in medium-heavy Ξ^- atoms. The dashed curves are for $b_0 = -0.25 + i0.04$ fm, i.e. a repulsive real potential.

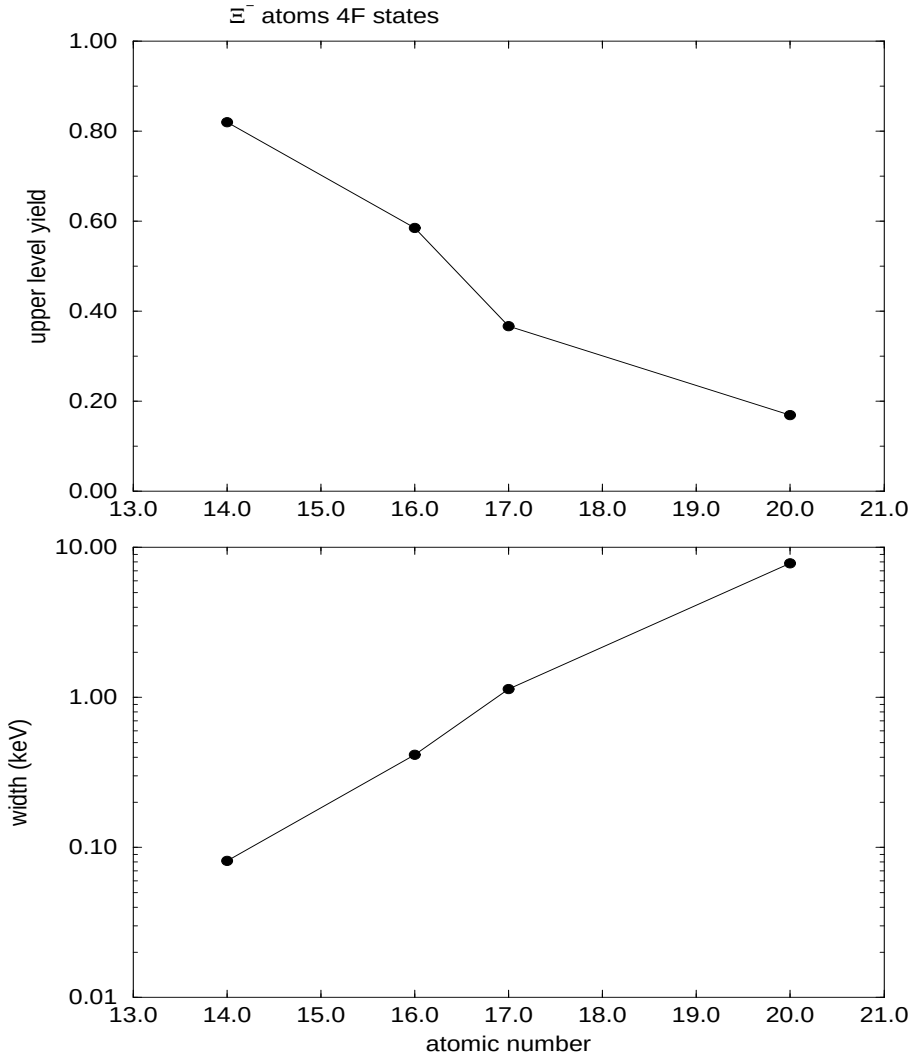

FIG. 5. Calculated strong interaction widths and upper level relative yields for the $4F$ level in Ξ^- atoms.

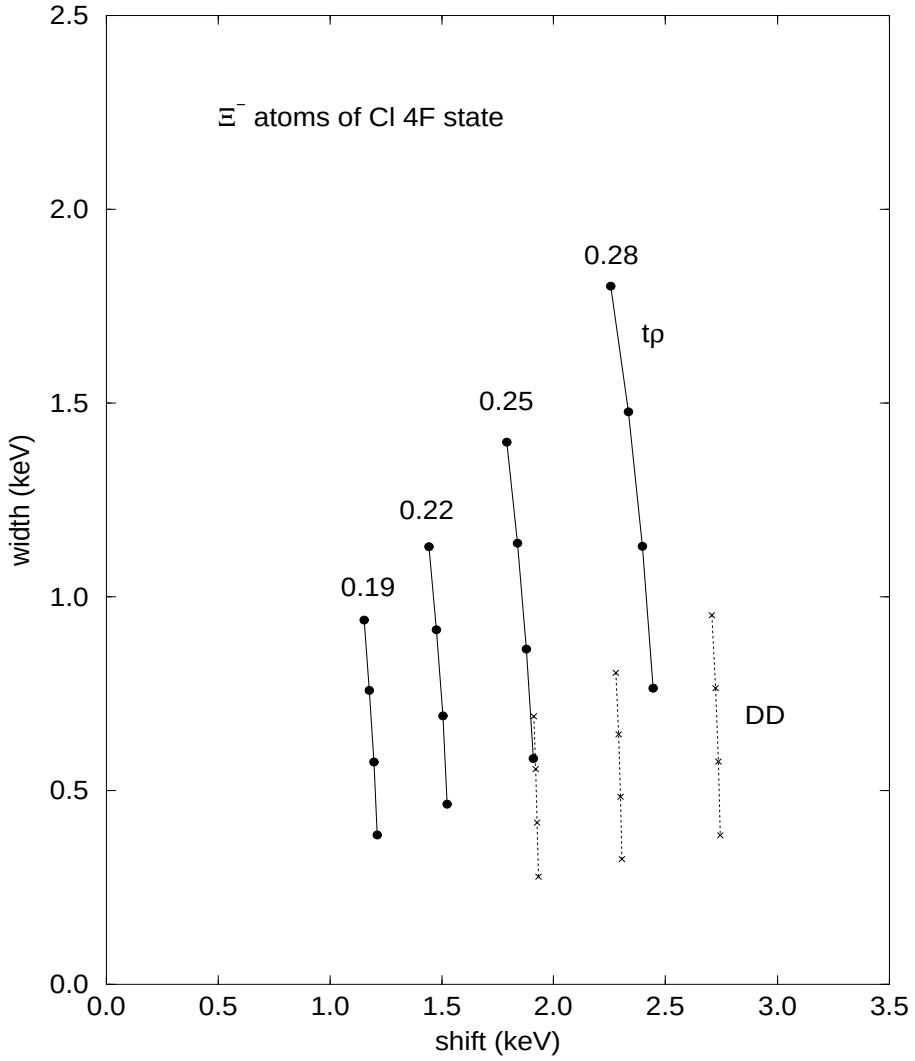

FIG. 6. Calculated strong interaction shifts and widths for the $4F$ level in Ξ^- atoms of Cl for different optical potentials, see text for detail.

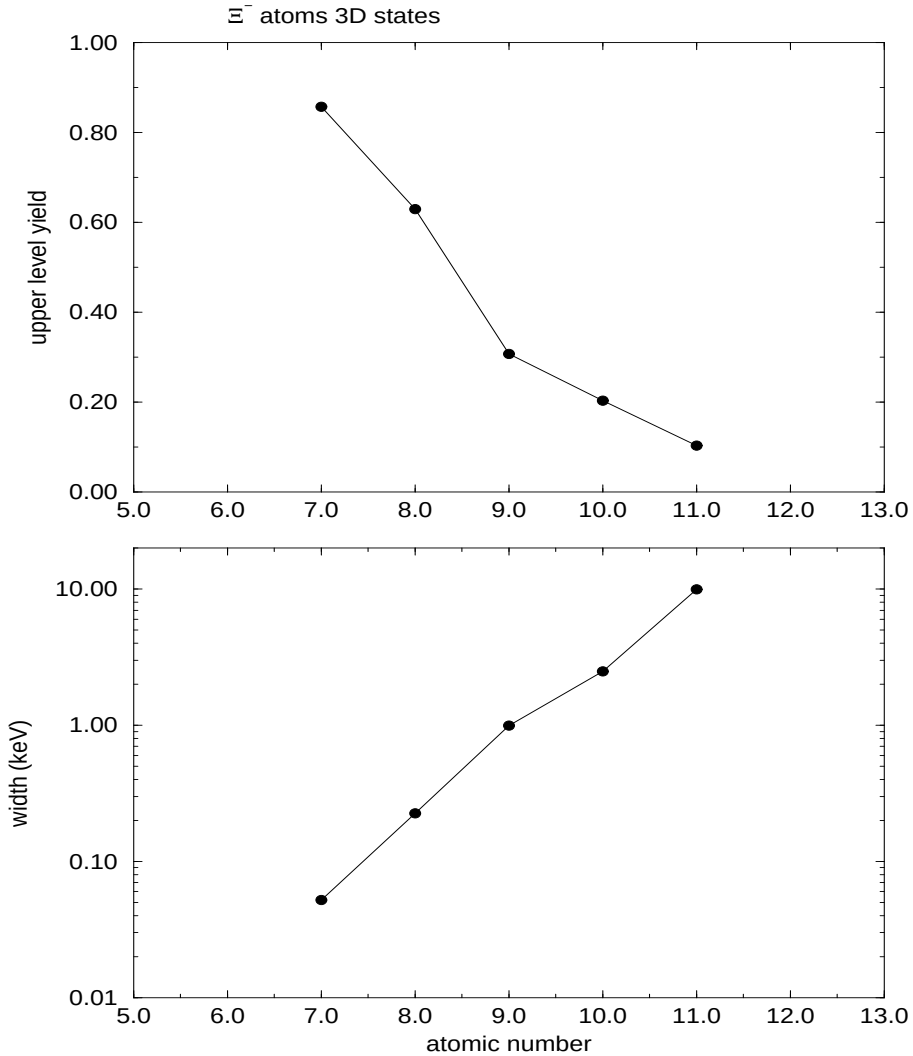

FIG. 7. Calculated strong interaction widths and upper level relative yields for the $3D$ level in Ξ^- atoms.

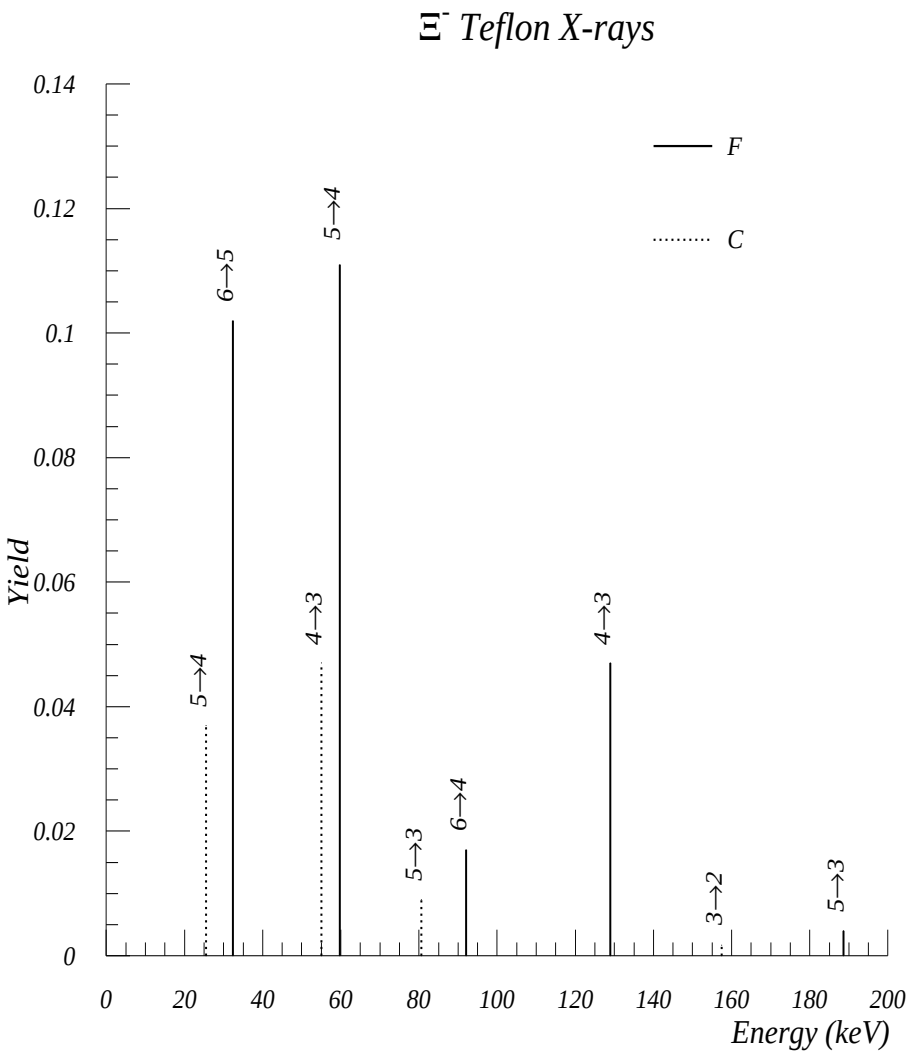

FIG. 8. Calculated X-ray spectrum for a teflon target.

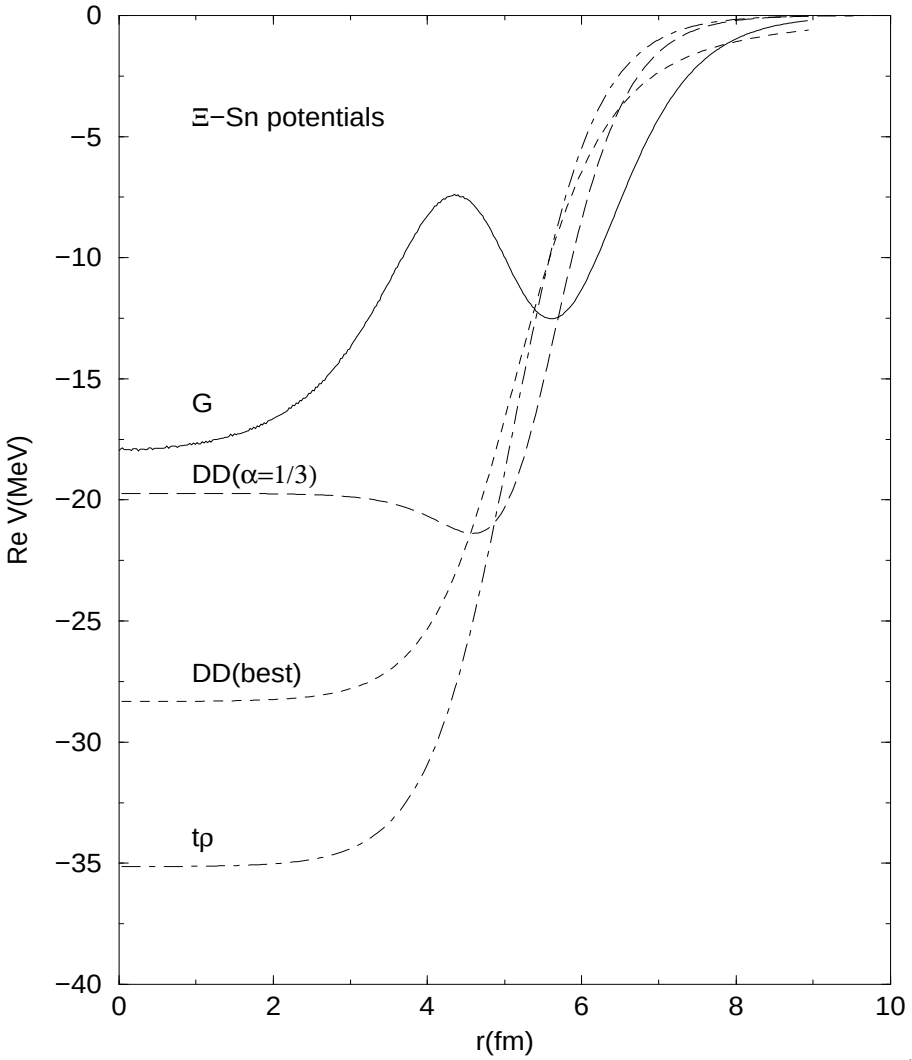

FIG. 9. Real optical potentials for Ξ interaction with Sn. Solid curve (G) is for Eq. (5) used to generate the 'pseudo data'. The other curves are the fitted potentials obtained under various constraints. See text.

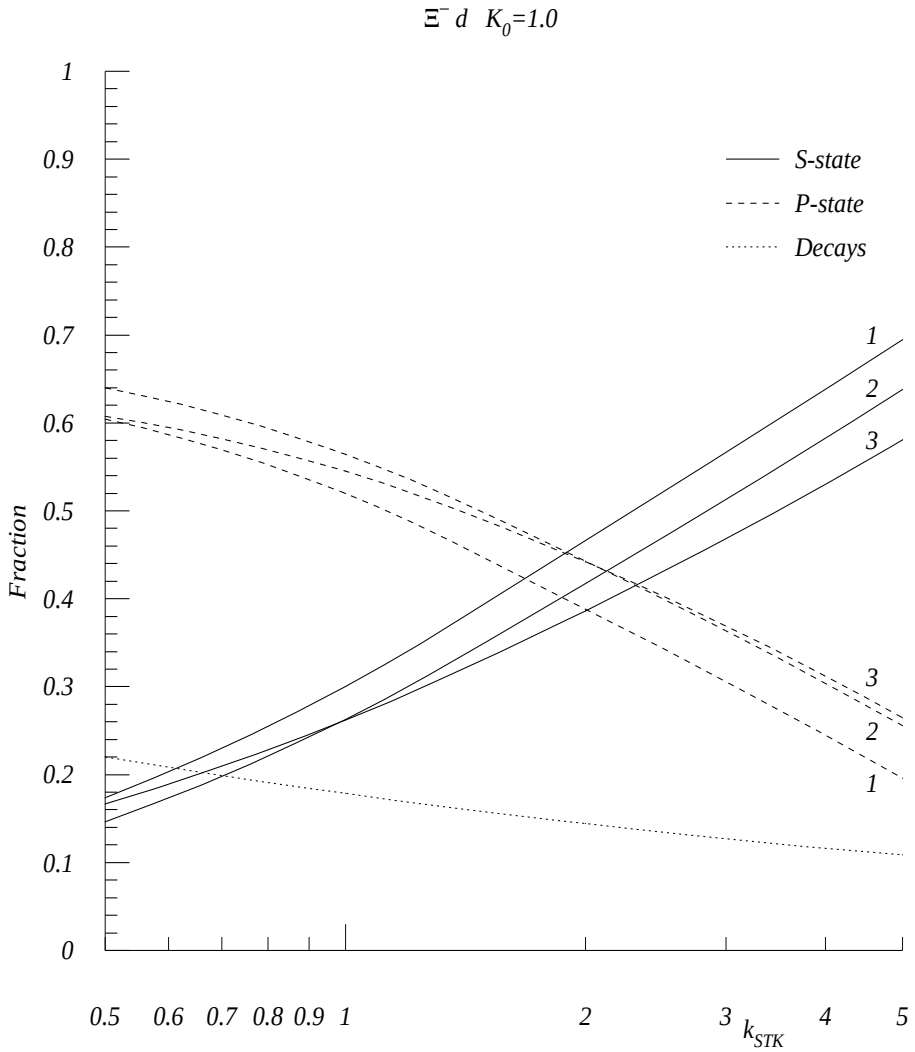

FIG. 10. Calculated fractions of S and P state capture, and of Ξ^- decays, for three choices of the strong interaction parameters Γ_{1S} and Γ_{2P} (see text) as a function of the Stark mixing parameter k_{STK}.

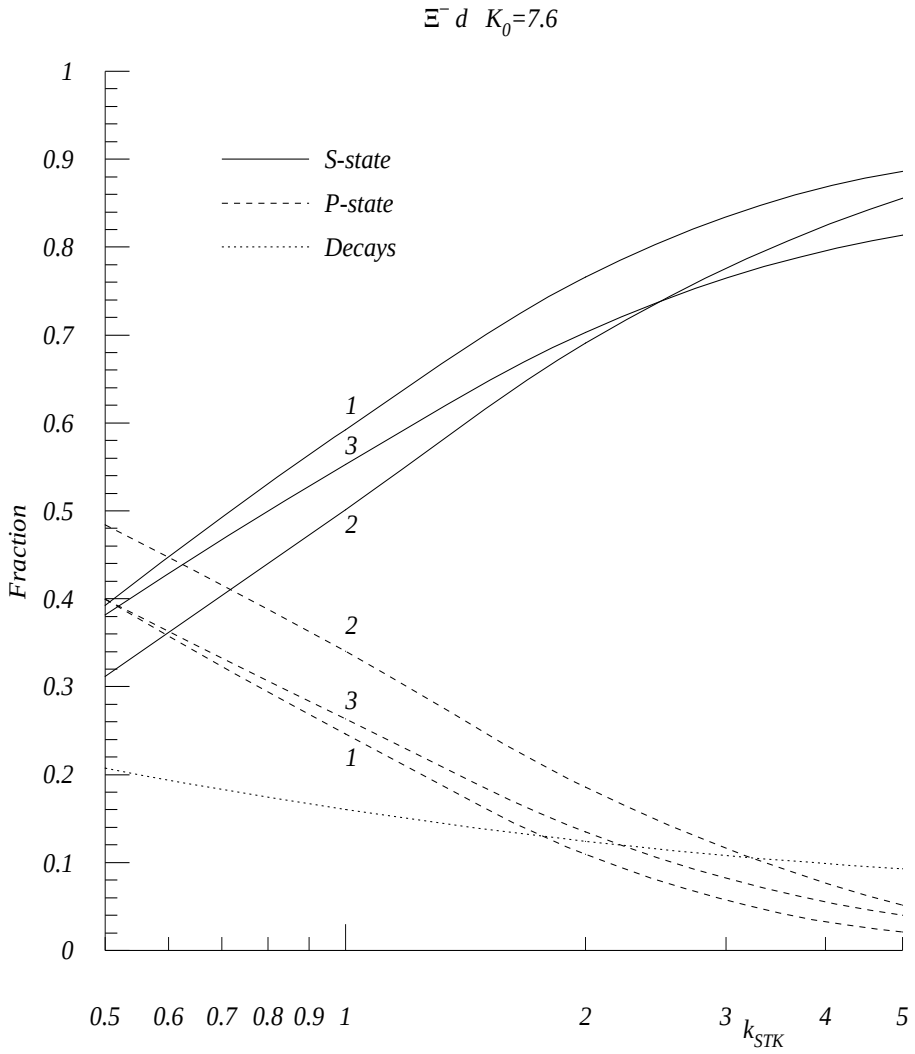

FIG. 11. Same as Fig. 10 but with the additional Stark mixing parameter $K_0 = 7.6$.

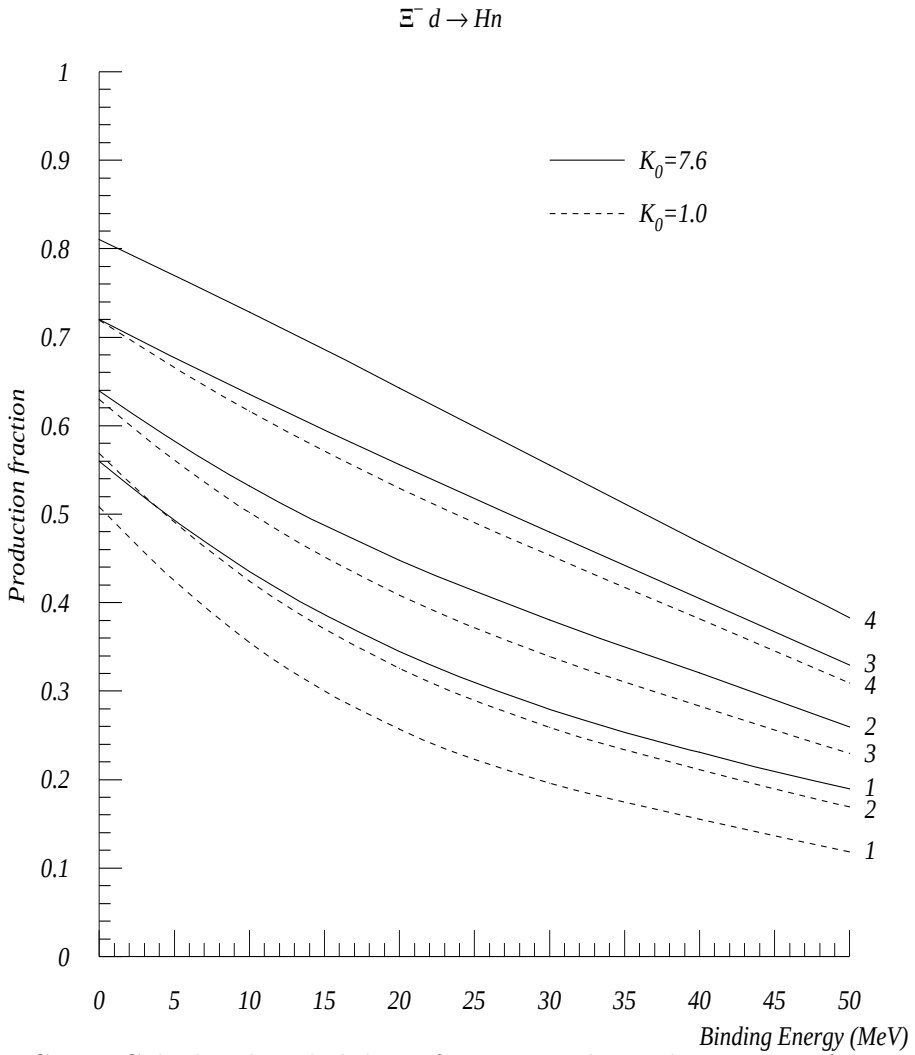

FIG. 12. Calculated probabilities for H particle production as a function of its binding energy $B(H)$. Curves labelled 1, 2, 3 and 4 correspond to values of the Stark mixing parameter k_{STK} = 0.5, 1.0, 2.0 and 5.0 respectively. The dashed and solid lines correspond to values of $K_0 = 1.0$ and 7.6 respectively. (See text).

TABLES

TABLE I. Calculated binding energies and strong interaction widths (in keV) of $3D$ Ξ^- atomic states.

	^{12}C	^{14}N	^{16}O
Coulomb only	126.36, Γ=0.000	174.71, Γ=0.000	230.90, Γ=0.000
potential 1	126.39, Γ=0.012	174.81, Γ=0.052	231.32, Γ=0.226
potential 2	126.38, Γ=0.010	174.78, Γ=0.040	231.17, Γ=0.167

TABLE II. Predictions for likely targets for a Ξ^- atoms experiment. Calculations are based on a $t\rho$ potential with $b_0 = 0.25 + i0.04$ fm. E_x is the transition energy, Y is the upper level relative yield.

target	F	Cl	Sn	I	Pb
transition	$4F \to 3D$	$5G \to 4F$	$8J \to 7I$	$8J \to 7I$	$10L \to 9K$
E_x (keV)	131.29	223.55	420.25	474.71	558.47
Y	0.31	0.37	0.76	0.43	0.58
shift (keV)	1.56	1.84	0.67	2.79	1.73
width (keV)	0.99	1.14	0.43	2.21	1.26

TABLE III. Parameters for the G-matrix interaction Eq. (4)

β_i (fm)	2.0	0.9	0.5
a_i (MeV)	−2.595	−200.7	821.4
b_i (MeV fm)	0.2632	63.94	−124.0

TABLE IV. Calculated shifts and widths (in keV) due to potential G, Eqs. (4,5) and Table III.

atom	O(3D)	F(3D)	S(4F)	Cl(4F)	Sn(7I)	I(7I)	W(9K)	Pb(9K)
shift	3.343	14.23	7.511	20.53	8.725	40.39	3.191	22.90
width	0.924	7.619	2.523	11.68	3.393	40.29	0.846	16.63